



Synthesis, Characterization, and Modeling of Reduced Graphene Oxide Supported Adsorbent for Sorption of Pb(II) and Cr(VI) Ions from Binary Mixture

Amina Kanwal¹ · Tayyaba Shahzadi² · Tauheeda Riaz¹ · Maria Zaib²

Received: 6 June 2024 / Accepted: 24 July 2024

© The Author(s), under exclusive licence to Springer Science+Business Media, LLC, part of Springer Nature 2024

Abstract

Graphene and its derivatives as multifunctional catalysts are in high demand, owing to their exceptional potential. Here, we synthesized Cu/Ni@rGO nanocomposite by using reduced graphene oxide (rGO) as a support which provided large surface area. A mixture of Cu and Ni nanoparticles (NPs) was embedded on its surface for sorption of heavy metal ions, i.e., Pb²⁺ and Cr⁶⁺, from binary mixture. Synthesis process of nanocomposite was monitored by UV-visible spectroscopy. FTIR analysis was performed to confirm the functional groups involved in synthesis and stabilization of the nanocomposite. The average size of nanocomposite was 26 nm calculated by XRD spectroscopy. SEM analysis revealed the thread-like structure of nanocomposite, while EDX gave information about elemental composition. Synthesized material was used to remove cations (Pb²⁺ and Cr⁶⁺) from binary mixture under tungsten lamp and without tungsten lamp. Under tungsten lamp, at 5 ppm concentration of binary mixture of cations, after 40 min of interaction with 10 mg adsorbent dosage at 45 °C temperature, 94% of cations was removed very efficiently. Thermodynamics studies showed that reaction of cations with nanocatalyst was spontaneous and exothermic in nature. Kinetics models were employed on experimental values and regression coefficient (R^2) was near to unity (0.99) for pseudo 2nd order, which was considered the best fitted method for adsorption. Among sorption isotherms, the best fitted model was Freundlich isotherm as its R^2 value (0.97) is near to unity. On these adsorption isotherms, error analysis was also applied to attain precision on results. Reusability of material was analyzed 5 times by desorption process which confirmed its stability and higher catalytic efficiency.

Keywords Cu/Ni@rGO nanocomposite · Pb²⁺ and Cr⁶⁺ contaminants · Thermodynamics · Sorption isotherms · Kinetics models

Introduction

Many environmental issues happen due to contaminated industrial wastewater [1]. Contaminated wastewater contains hazardous organic and inorganic pollutants. Untreated and less treated water contain such contaminants which are added into the food chains and thus destroy the cleanliness of an ecosystem [2]. The level of such unhealthy environment is increasing

day by day because of increase in population and not paying serious intention to cleanliness of the environment [3, 4].

Chromium is present in soil, plants, and water due to both natural and artificial sources. It is found as chromium ore like chromium-iron minerals in natural resources, while anthropogenic sources include dying, plastic industries, steel industry, batteries, metallurgy, and galvanized pipes [5]. The presence of chromium ions in natural water resources can cause cancer and hazardous health effects on the kidneys, bones, lungs, liver, brain, cardiovascular system, and immunological system [6, 7].

Lead is present in lead-based batteries, alloys, solder, rust inhibitors, cable sheathing pigments, ammunition, plastic stabilizers, and glaze [8, 9]. From all these sources, lead is being added into natural environment which causes adverse effects on the bones, kidneys, liver, lungs, brain, spleen, hematological system, immunological system, reproductive system, and cardiovascular system [10].

✉ Tayyaba Shahzadi
tayyaba332@gmail.com; tayyaba.shehzadi@gcwus.edu.pk

¹ Department of Chemistry, Government College for Women University Sialkot, Sialkot 51310, Pakistan

² Department of Chemistry, University of Jhang, Jhang 35200, Pakistan

Permitted amounts of lead (0.01 mg/L) and chromium (0.05 mg/L) are allowed in water by the World Health Organization (WHO) to avoid their toxic effects on health. But above the limited amount, they can cause serious health issues in animals [11, 12].

To remove these contaminants from water, various conventional techniques are being used like ion exchange, chemical precipitation, membrane filtration, electrochemical treatment, and coagulation/flocculation [13]. Due to their lower efficiency and large amount of waste, an alternative method has been searched [14]. The best alternative method is sorption in which an adsorbent is used to remove contaminants from water [15]. Actually, sorbate transfers from water to the sorbent surface, and during this transfer, different factors were optimized like temperature, pH, initial concentration of metals, and adsorbent dosage [16].

Different types of sorbents have been used in adsorption mechanism including nanomaterials [17]. Nanomaterials can be functionalized by adding some supporting material like graphene. By adding graphene-like materials, the characteristics of the nanocomposites can be enhanced and thus nanomaterials are considered as the best adsorbent material to remove contaminants from the wastewater [18, 19].

Nanomaterials in composite form can show excellent catalytic properties in adsorption mechanism. Generally, a composite is formed when two materials in the same phase or different phases join together [20]. Graphene having distinctive arrangements in its structure shows extraordinary properties. Due to its unique properties, it is used as supporting material in nanocomposites [21]. Graphene has maximum adsorption capacity because of the presence of substantial number of negatively charged oxygen groups on it, so it adsorbs various cations such as copper (Cu(II)) [22], lead (Pb(II)) [23], cobalt (Co(II)) [24], chromium (Cr(VI)) [25], and cadmium (Cd(II)) [26]. But due to strong inter-functional bond between graphene sheets leads to decreased surface area, inactive surface chemical properties, agglomeration and poor dispersion in aqueous media, decreasing its adsorption ability [27].

To improve the removal efficiency, the graphene can be modified to reduced graphene oxide (rGO), hence converting carboxyl groups into hydroxyl groups. rGO has more surface area as compared to graphene [28]. GO-based materials including fabrication of GO/metal oxide composites [29], chemical modification of GO [30], GO/photocatalytic composites [31], and GO/organic compound composites [32] have been used efficiently to remove different heavy metal ions from wastewater. Recent studies have explored such material in which graphene is used as supporting material to enhance the catalytic properties of the material [33, 34]. Metals in the structure of graphene material enhanced the mechanical, electrical, and thermal properties [35].

Here, reduced graphene oxide-based nanocomposite was prepared by phytoconstituents (ricinine, quercetin, rutin, and kaempferol) present in aqueous extract of *Ricinus communis* leaves, which reduced the Cu/Ni metals and stabilized the nanocomposite [36]. The synthesized nanocomposite (Cu/Ni@rGO) was used for simultaneous removal of Pb²⁺ and Cr⁶⁺ contaminants from binary mixture by optimizing different factors. Thermodynamics, kinetics, and adsorption isotherms were applied on experimental data. To analyze the best fitted isotherm model, error analysis was also performed. Reusability of Cu/Ni@rGO nanocomposite was analyzed that proves the efficiency of material.

Prior to the current investigation, *Ricinus communis* leaves have not been employed in the synthesis of Cu/Ni@rGO nanocomposites. This method offers a cost-effective and swift method for efficiently removing cations from binary mixture.

Experimental Section

Materials and Reagents

Reagents used in the experimental work were CuCl₂ (copper chloride), NiCl₂ (nickel chloride), graphite powder, KMnO₄ (potassium permanganate), H₂SO₄ (sulfuric acid), H₂O₂ (hydrogen peroxide), Pb(NO₃)₂ (lead nitrate), and K₂Cr₂O₇ (potassium dichromate), purchased from Sigma-Aldrich.

Formation of Plant Extract

Plant (*Ricinus communis*) was collected from local areas of Sialkot, Pakistan. After careful washing with water, it was left to dry under the shade and then transformed into a fine powder. Three grams of powdered plant was added into 100 mL of distilled water in a beaker. Mixture was kept on hot plate and temperature was set at 70 °C for 45 min. The resulting plant extract was cooled down to room temperature, filtered, and filtrate was stored at room temperature for further experiments [37, 38].

Synthesis of Graphene Oxide (GO)

Modified Hummer's method was utilized to form graphene oxide [39, 40]. The process was completed in the following six steps.

- (I) The process was initiated by adding 1 g of graphite powder into 25 mL concentrated sulfuric acid (H₂SO₄) in a 1000 mL beaker, with vigorous stirring in an ice bath.
- (II) Afterward, 3 g of KMnO₄ (potassium permanganate) was slowly added to the reaction mixture.

With continuous stirring for about 3 h, 50 mL of distilled water was gradually added drop by drop. During this reaction, temperature was maintained below 50 °C.

- (III) In the next step, 100 mL distilled water was added into the reaction mixture at once.
- (IV) To convert unreacted MnO_4^- ions into MnO_2 , 5 mL of H_2O_2 (hydrogen peroxide) was added.
- (V) Excess acid was eliminated by multiple washings with distilled water.
- (VI) Residual product was obtained by centrifugation and was then dried by placing it in an oven at 60 °C for about 24 h.

Formulation of Cu/Ni@rGO Nanocomposite

Cu/Ni@rGO nanocomposite was synthesized in a single step by adding 1.0 g of dried graphene oxide (GO) into 100 mL of plant extract in a glass beaker. Reaction mixture was kept on hot plate and heated at 80 °C along with continuous stirring. After 10 min, 20 mL of CuCl_2 (0.05 M) solution and NiCl_2 (0.05 M) were added into the reaction mixture. Reaction time was kept about 8 h for the complete synthesis of nanocomposite.

Characterization Techniques

UV-Vis. Spectrophotometer (Specord 210 Plus, Analytik Jena AG, Germany), Fourier transform infrared spectroscopy (FTIR, Thermo Scientific Nicolet 6700), X-ray diffraction (XRD, JEOL, Neoscope, JCM-600), scanning electron microscope (SEM), and energy-dispersive X-ray spectroscopy (EDX) (Vega LMU, TESCAN, Czech Republic) were used to characterize the Cu/Ni@rGO nanocomposite. Confirmation of the synthesis, morphology, size of particles, and structural and elemental composition was analyzed through these techniques.

Point of Zero Charge Determination

Salt addition method was used to find out the point of zero charge of synthesized nanocomposite [41]. 0.1 M NaNO_3 solution was prepared and pH was adjusted as 2, 3, 4, 5, 6, 7, 8, 9, 10, 11, and 12 by using 0.1 M HCl and NaOH in series of beakers. 10 mg of adsorbent was added to each of above solution (25 mL). Reaction was allowed to complete for 24 h on orbital shaker. After that, pH of these solutions was monitored which was considered as pH_f . A graph was plotted against ΔpH ($\text{pH}_i - \text{pH}_f$) and pH_i . Crossing point at the X-axis was considered the point of zero charge on synthesized nanocomposite [42, 43].

Adsorption, Thermodynamics, Kinetics, and Isotherm Studies of Cations (Pb^{2+} and Cr^{6+})

Thermodynamics, isotherm models, and kinetics studies were performed to analyze the removal of cations in a single step by the synthesized nanocomposite (Cu/Ni@rGO).

Standard solution of 1000 mg/L of both cations (Pb^{2+} and Cr^{6+}) was prepared separately. Equal proportion (25 mL) of each of these solutions was taken to prepare the binary system. Percentage removal of cations was calculated by the following formula.

$$\% \text{ Removal} = \frac{C_i - C_f}{C_i} \times 100 \quad (1)$$

Here, C_i and C_f are considered the initial and final concentration of metal ions in the solution, respectively. During removal mechanism, different parameters (temperature, pH, adsorbent dosage, and initial concentration of metal ions) were optimized for maximum removal of ions from binary system.

Thermodynamics

To calculate the thermodynamic parameters, i.e., ΔH° , ΔS° , and ΔG° , the following formulas were used.

$$\Delta G^\circ = -RT \ln K_c \quad (2)$$

$$K_c = C_{\text{ad}}/C_e \quad (3)$$

$$\ln K_c = \Delta S^\circ / R - \Delta H^\circ / RT \quad (4)$$

In the above equations, T is indicating the temperature in Kelvin scale, R is used as general gas constant, and K_c is the equilibrium constant.

Kinetics Models

The following equations were used to calculate the constant values of both models, i.e., pseudo 1st order and pseudo 2nd order model.

$$\ln(q_e - q_t) = \ln q_e - k_1 t \quad (5)$$

$$t/q_t = 1/k_2 q_e^2 + t/q_e \quad (6)$$

In both equations, q_e is the amount of contaminant adsorbed on catalytic surface at equilibrium and q_t is the amount of adsorbent at time t . K_1 is used as rate constant for pseudo 1st order model and k_2 is for pseudo 2nd order.

Isotherm Models

Linear forms of Langmuir equation:

$$1/q_e = 1/K_L q_m \times 1/C_e + 1/q_m \quad (7)$$

where q_m was used for monolayer formation capacity of adsorbed molecules and K_L denotes the binding nature of adsorbed species on catalytic surface of synthesized nanocomposite. K_L value was used in calculation of separation factor R_L that predicted the affinity of adsorbed species on adsorbent. To calculate R_L value, the following formula is used.

$$R_L = 1/I_1 + KIC_I \quad (8)$$

Freundlich isotherm assumed the multilayer adsorbent formation with non-uniform energy distribution.

$$\log q_e = \log K_f + 1/n \log C_e \quad (9)$$

where n and K_f are Freundlich constants.

The Temkin isotherm equation is expressed as

$$q_e = RT/B\ln(K_T) + RT/B\ln(C_e) \quad (10)$$

Equation used for Temkin isotherm gave calculated values of B that corresponds to the heat sorption constant. R denoted the general gas constant and T was the temperature in Kelvin scale.

Results and Discussion

Phytoconstituents of *Ricinus communis* like ricinine, quercetin, rutin, and kaempferol in aqueous extract were responsible for metal ion (Cu^{2+} and Ni^{2+}) reduction to form stable nanocomposite [44, 45].

Characterization

During UV-visible spectroscopy, electromagnetic radiations fell on nanocomposite; as a result, electron moved from valence band to the conduction band and absorption peaks appeared [46]. The absorption peaks of GO were observed at 233 nm and 300 nm which was due to the aromatic C–C bond of π - π^* transition and the C=O of the n - π^* transition (Fig. 1) [17]. After the reduction treatment, the UV-visible absorption spectra of Cu/Ni nanoparticles decorated rGO exhibited a new peak in the range of 200–400 nm due to the surface plasmon resonance effect of Cu/Ni nanoparticles which confirmed the formation of Cu/Ni@rGO nanocomposite. When nanocomposite spectrum was compared with graphene spectrum, the nanocomposite peak showed a slight

shifting of peak between 200 and 400 nm. No any additional peak was recorded in spectrum of Cu/Ni@rGO nanocomposite which corresponded to its high purity [47].

Fourier transform infrared spectroscopy was used to determine functional groups [48]. The FTIR spectrum of GO and synthesized nanocomposite Cu/Ni@rGO (Fig. 2a, b) was taken in the range of 500–4000 cm^{-1} . Spectrum of GO depicted 4 peaks due to stretching vibrations of C–O, C=O, and OH functional groups at 697 cm^{-1} , 1541.75 cm^{-1} , 1575.36 cm^{-1} , and 2988.03 cm^{-1} , respectively.

Cu/Ni@rGO nanocomposite (Fig. 2b) showed multiple peaks as compared to GO spectrum. Two new peaks at 3240.58 cm^{-1} and 2831.72 cm^{-1} were due to stretching vibrations of OH functional groups. Many new peaks toward lower intensity were actually due to the shifting of 1541.75 cm^{-1} peak toward 1575.36 cm^{-1} due to C=O stretching vibrations. The peak at 697 cm^{-1} moved toward 930.54 cm^{-1} denoting C–O vibrations. Shifting and appearance of new peaks confirmed the formation of synthesized nanocomposite [49–51].

To calculate the size of nanomaterial and its structural properties, X-ray diffraction spectroscopy was performed [37]. Here, the synthesized nanocomposite Cu/Ni@rGO was analyzed (Fig. 3) and size was calculated by the Debye-Scherrer equation:

$$D = \frac{K\lambda}{\beta \cos\theta} \quad (11)$$

Here, K is the proportionality constant and its value is 0.9. β is denoting the full width at half maximum. λ is the wavelength of X-rays and θ is the Bragg angle.

Intense peaks in the XRD spectrum always correspond to the crystalline nature of the material [52]. Spectrum of synthesized material showed 5 intense peaks ($2\theta = 25.68$,

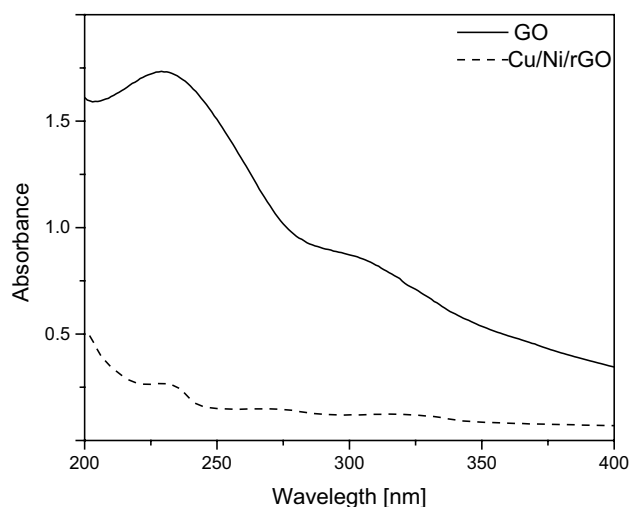


Fig. 1 UV-visible spectrum of Cu/Ni@rGO nanocomposite

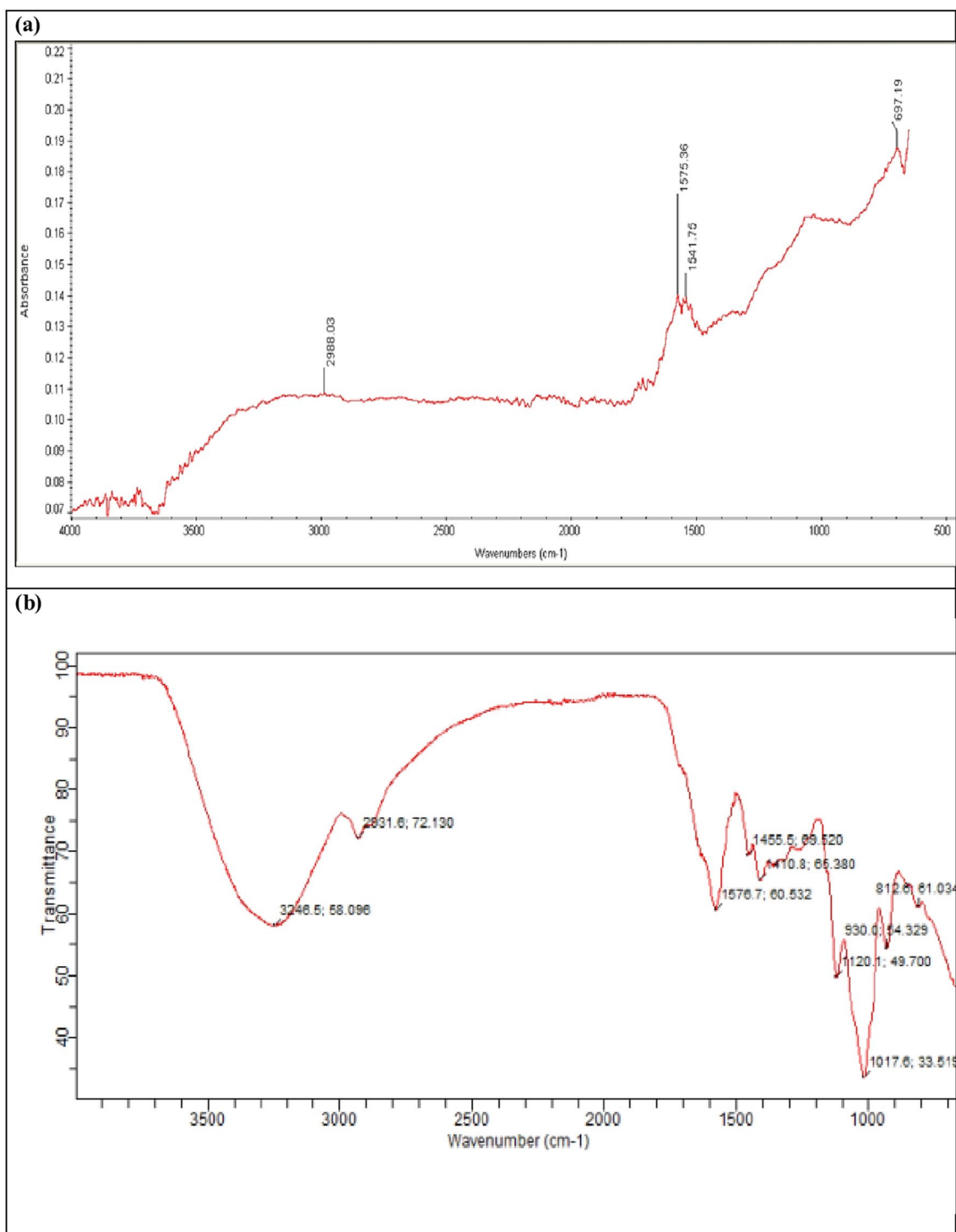


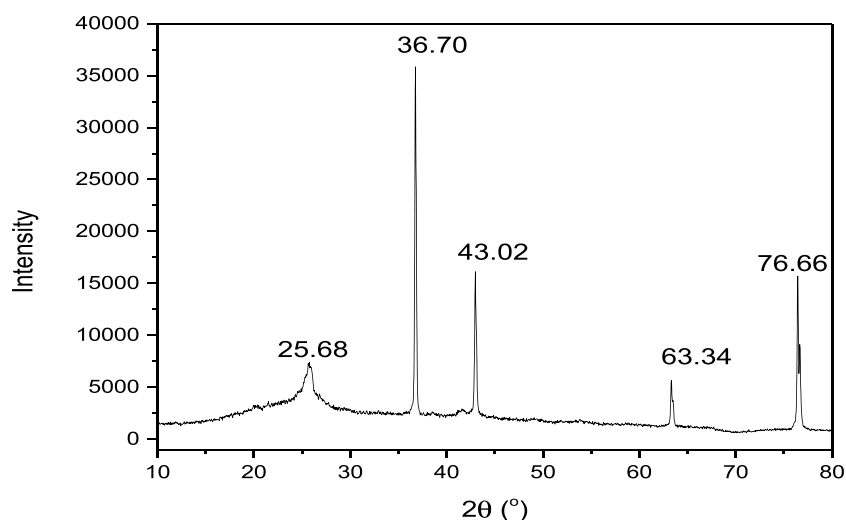
Fig. 2 FTIR spectrum of **a** GO and **b** Cu/Ni@rGO nanocomposite

36.07, 43.02, 63.34, 76.66) that confirmed the crystalline nature of nanomaterial, and by using the data obtained from peaks, average size calculated was found to be 26 nm.

Scanning electron microscopy was employed to get information about surface morphology [53]. SEM images

were taken at different resolution of 1 μm , 3 μm , and 5 μm (Fig. 4a–c). Clusters of nanocomposite were formed due to polymeric nature and thread-like structure of synthesized material, confirmed by SEM analysis that corresponded to high surface area of catalytic material [54]. SEM images of

Fig. 3 XRD spectrum of Cu/Ni@rGO nanocomposite



Cu/Ni@rGO after adsorption of lead and chromium ions are seen in Fig. 4d–f. Cracks in Fig. 4d image correspond to the roughness of surface that was due to the adsorbed species on the surface. Agglomeration in Fig. 4e presented the enhanced surface area and reactivity of the material, and Fig. 4f shows the adsorbed species on surface of the material that describe about surface coverage with lead and chromium metal ions [55].

Elemental composition and purity of the synthesized composite were confirmed by energy-dispersive X-ray spectroscopy [56]. The EDX image of Cu/Ni@rGO is shown in Fig. 5 which confirmed the high purity of synthesized material. The spectrum was taken in the range of 0–5 keV and peaks of O, Cu, and Ni were examined.

Point of Zero Charge

By knowing the charge on the surface of nanocomposite, it can be made possible to attain the condition where maximum removal of contaminants will occur. During this study, point of zero charge was measured by salt addition method and it was found as 6.5 which is nearly neutral (Fig. 6). The surface of nanocomposite can be made positive by lowering the pH value and negative by increasing the pH value, for maximum removal of cations.

Factor Optimization

Adsorbent Dosage

To analyze the effect of amount of nanocatalyst, different dosages (5 mg, 10 mg, 20 mg, 40 mg, and 60 mg) were added into separate beakers along with 25 mL (5 ppm) of binary mixture of cations (Pb^{2+} and Cr^{6+}). Experiment was

performed under tungsten lamp and without tungsten lamp. Tungsten lamp source subsidized the separation of charges and decreased recombination rates; therefore, maximum % removal was seen under tungsten lamp. However, the trend of % removal of cations remains the same under tungsten lamp and without tungsten lamp. % Removal was observed like 93% for Pb^{2+} and 95% for Cr^{6+} under tungsten lamp, and without tungsten lamp, it was 70% for Pb^{2+} and 67% for Cr^{6+} . This pattern of % removal was observed due to the reason that fixed amount of nanocatalyst can adsorb a limited amount of ions according to its surface area. It was seen that maximum removal was up to a certain limit and after that decrease in % removal was observed (Fig. 7a, b). The reason behind this decreasing trend was aggregation of ions on Cu/Ni@rGO nanocatalyst surface. Accumulation of ions occurred due to excess amount that led to lower % removal [57, 58].

Effect of Initial Concentration

Different concentrations of cations (5 ppm, 10 ppm, 25 ppm, 75 ppm, and 100 ppm) were prepared to analyze the initial concentration effect on adsorption mechanism. Fixed amount of nanocatalyst, i.e., 10 mg, was added into binary mixture (25 mL) and kept on stirring for about 2 h. The same experiment was performed twice under tungsten lamp and without tungsten lamp. Removal of both cations was in inverse relation with initial concentration of ions. Maximum removal was seen at lower initial concentration. The reason behind this trend was the maximum availability of active sites of nanocatalyst at lower ions' concentration. At higher concentration, active sites were already occupied and thus decreasing trend was observed (Fig. 8a, b). Without tungsten lamp, % removal of Pb^{2+} was 72% and Cr^{6+} was 70%, but under tungsten lamp, it was 94% for Pb^{2+} and 96% for Cr^{6+} [59, 60].

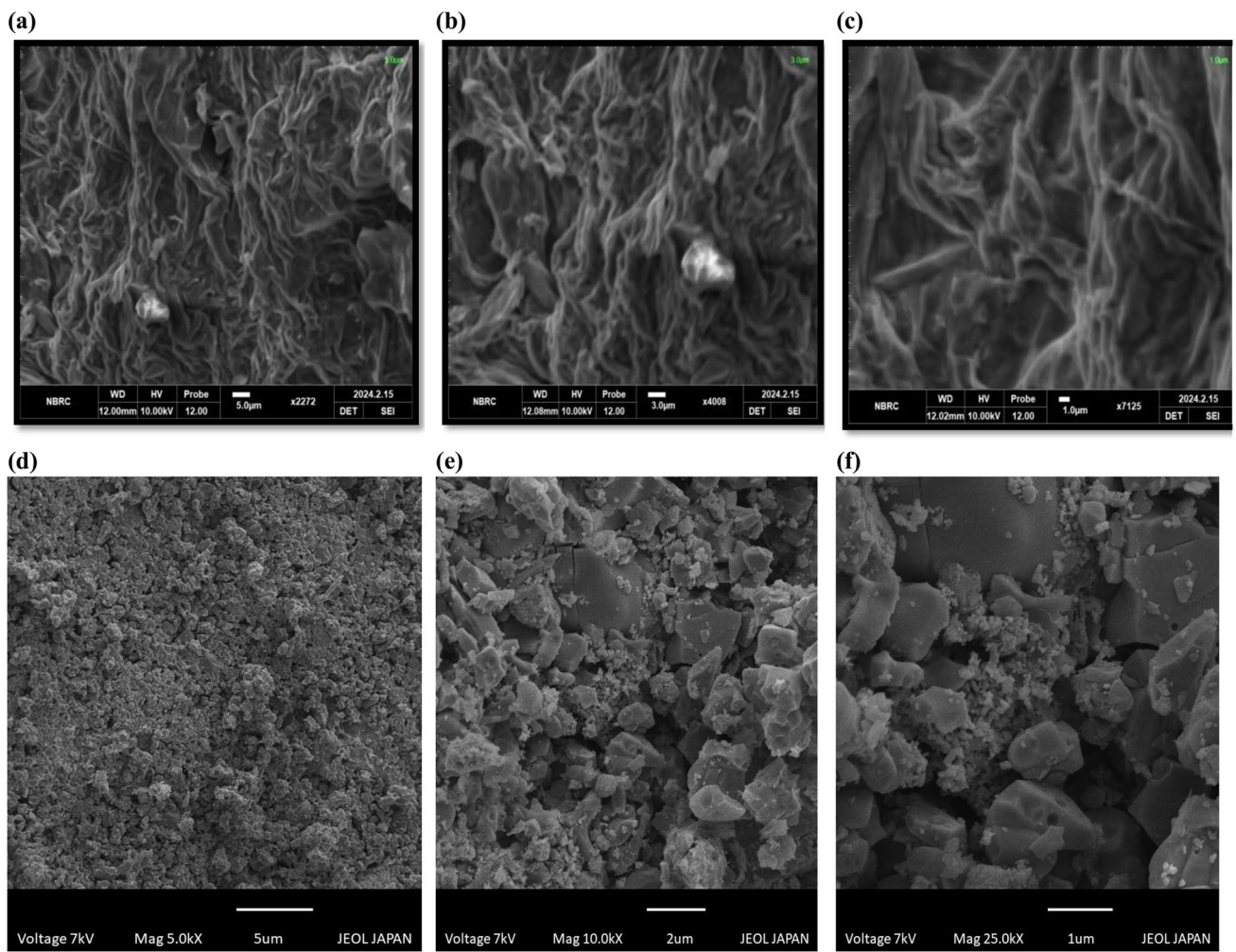
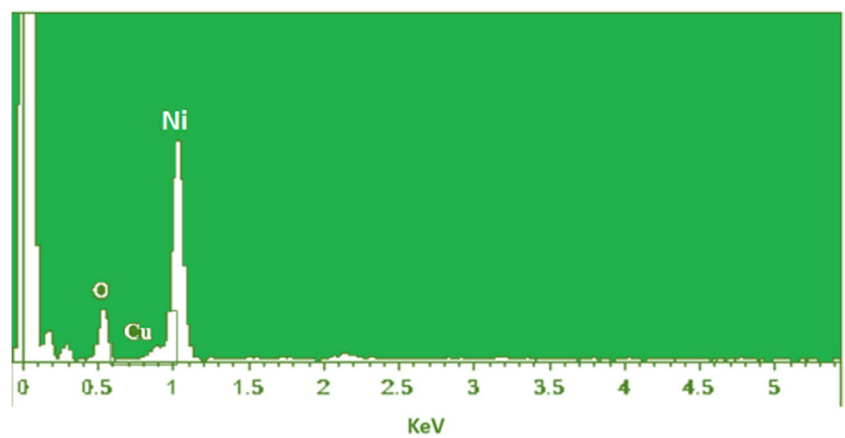


Fig. 4 SEM images of Cu/Ni@rGO nanocomposite before adsorption (a–c). SEM images of Cu/Ni@rGO nanocomposite after adsorption (d–f)

Fig. 5 EDX images of Cu/Ni@rGO nanocomposite



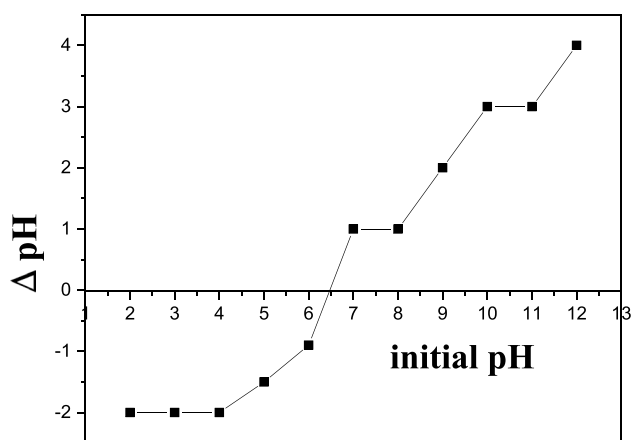


Fig. 6 Point of zero charge by salt addition method of Cu/Ni@rGO nanocomposite

Effect of Temperature

By setting different temperatures (25 °C, 35 °C, 45 °C, 55 °C, and 65 °C), maximum % removal of both cations was observed (Fig. 9a, b) under tungsten lamp and without tungsten lamp. Results concluded that at 45 °C both cations (Pb^{2+} and Cr^{6+}) showed maximum % removal.

Without tungsten lamp, it was 82% and 86% for Pb^{2+} and Cr^{6+} , respectively, while under tungsten lamp % removal was increased up to 95% for Pb^{2+} and 96% for Cr^{6+} . By increasing temperature K, E was also increased and thus more cations adsorb on the catalytic surface of adsorbent (Cu/Ni@rGO). % Removal of cations was increased up to 45 °C; then, equilibrium was established and no more % removal was observed [61, 62].

Effect of pH

Surface properties of any composite play an important role to remove contaminants. Here, the synthesized composite Cu/Ni@rGO was nearly neutral but its surface can be made negative or positive by changing pH of the solution mixture. Conditions were set by taking fixed amount of nanocatalyst, i.e., 10 mg of adsorbent, 25 mL binary mixture of cations while the pH range was kept between 2 and 12. As opposite charges attract, when the pH was higher and more negative charges (OH^-) were present on the catalytic surface of composite, maximum cations having positive charges adsorb on the surface. Lead (Pb^{2+}) showed maximum removal at pH 8, i.e., 65% without tungsten lamp and 91% under tungsten lamp. Chromium (Cr^{6+}) showed maximum % removal at pH 2 which decreased

Fig. 7 Effect of adsorbent dosage on binary mixture of cations on % removal by Cu/Ni@rGO nanocomposite **a, b** without tungsten lamp and **c, d** under tungsten lamp

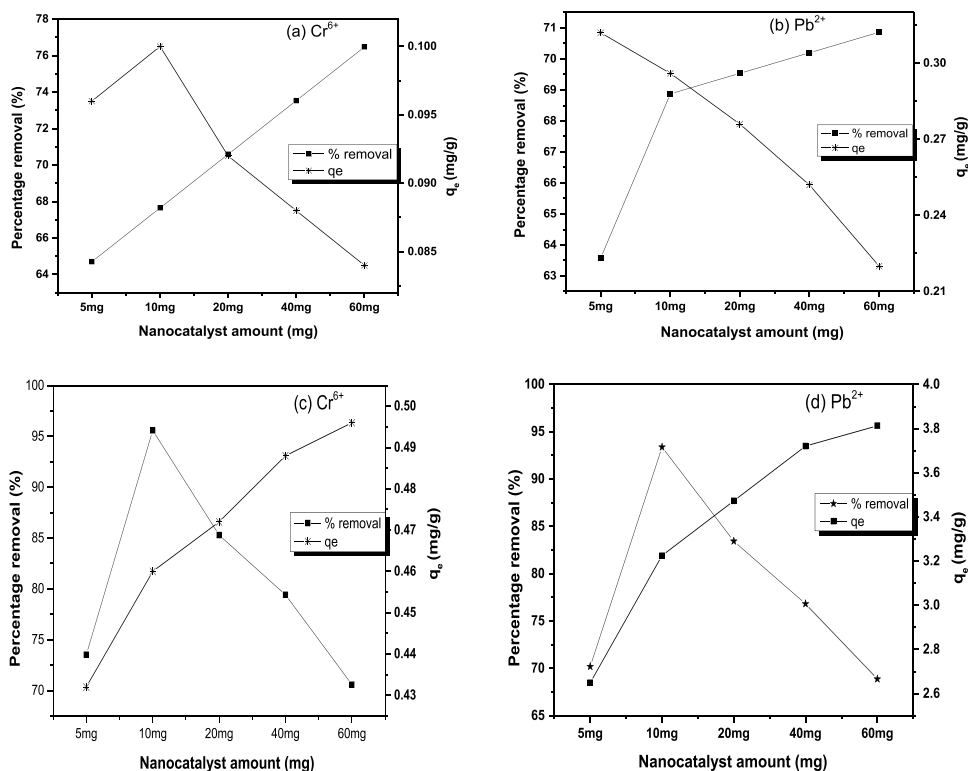


Fig. 8 Effect of initial concentration of binary mixture of cations on % removal by Cu/Ni@rGO nanocomposite **a** without tungsten lamp and **b** under tungsten lamp

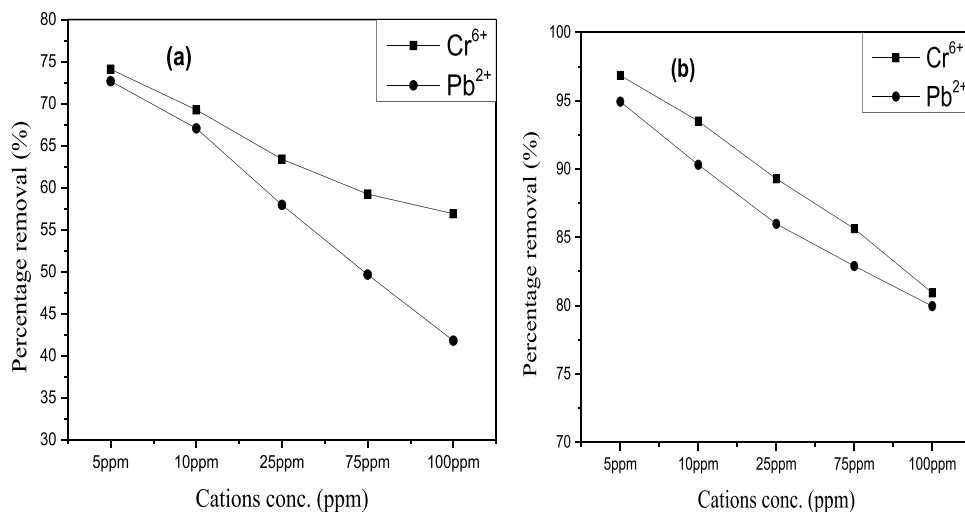
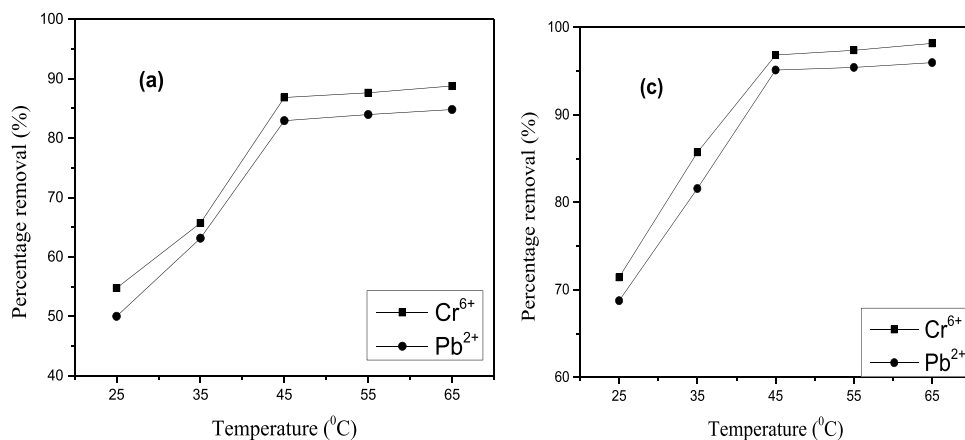


Fig. 9 Effect of temperature of cations on % removal by Cu/Ni@rGO nanocomposite **a** without tungsten lamp and **b** under tungsten lamp



rapidly with increasing pH value (Fig. 10a, b). Without tungsten lamp, % removal was 76% while under tungsten lamp it was 92%. Actually, at lower pH, anionic species of chromium (HCrO_4^- , $\text{Cr}_2\text{O}_7^{2-}$, $\text{Cr}_4\text{O}_{13}^{2-}$, $\text{Cr}_3\text{O}_{10}^{2-}$) were present in water. Among these species, HCrO_4^- has the lowest adsorption energy so it was more favorable species that adsorbed on catalytic surface of synthesized nanocomposite [63, 64].

Effect of Contact Time

To analyze the maximum removal efficiency of synthesized nanocomposite, time factor was also studied for contact time of 2 h by keeping other factors constant. Optimum time taken by the adsorbent to remove maximum number of contaminants from water can prove its efficiency. Here, the optimum time was 40 min recorded from Fig. 11a, b. Pattern of % removal of cations was the same but with different percentages. Without tungsten lamp, % removal of lead (Pb^{2+}) was 72% and chromium (Cr^{6+}) was 70%, while under tungsten

lamp % removal of lead (Pb^{2+}) was 94% and chromium (Cr^{6+}) was 96% recorded. After 40 min where maximum % removal was recorded, an equilibrium was established between adsorbent and adsorbate; hence, a slightly decreasing trend was observed when no more spaces remain left on catalytic surface for adsorption of contaminants [65, 66].

UV-visible spectrum of lead solution along with its spectrum after removal by Cu/Ni@rGO nanoadsorbent has been given in Supplementary Material (S1).

Thermodynamics

Adsorption mechanism in which the adsorbed species interact with nanoadsorbent was well explained with thermodynamic parameters [67].

Enthalpy change (ΔH) and entropy change (ΔS) were calculated from a linear plot of $\ln K_d$ versus $1/T$ as depicted in Fig. 12a, b. Values from these formulas were calculated and mentioned in Tables 1 and 2 which showed that the

Fig. 10 Effect of pH on cations on % removal by Cu/Ni/rGO nanocomposite **a** without tungsten lamp and **b** under tungsten lamp

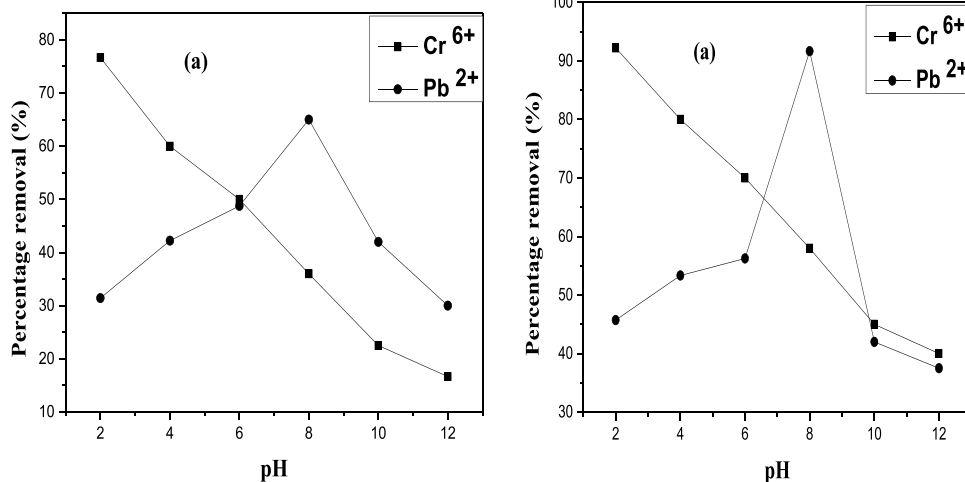


Fig. 11 Effect of time of Cr⁶⁺ on % removal by Cu/Ni@rGO nanocomposite **1a** without tungsten lamp and **1b** under tungsten lamp. Effect of time of Pb²⁺ on % removal by Cu/Ni@rGO nanocomposite **2a** without tungsten lamp and **2b** under tungsten lamp

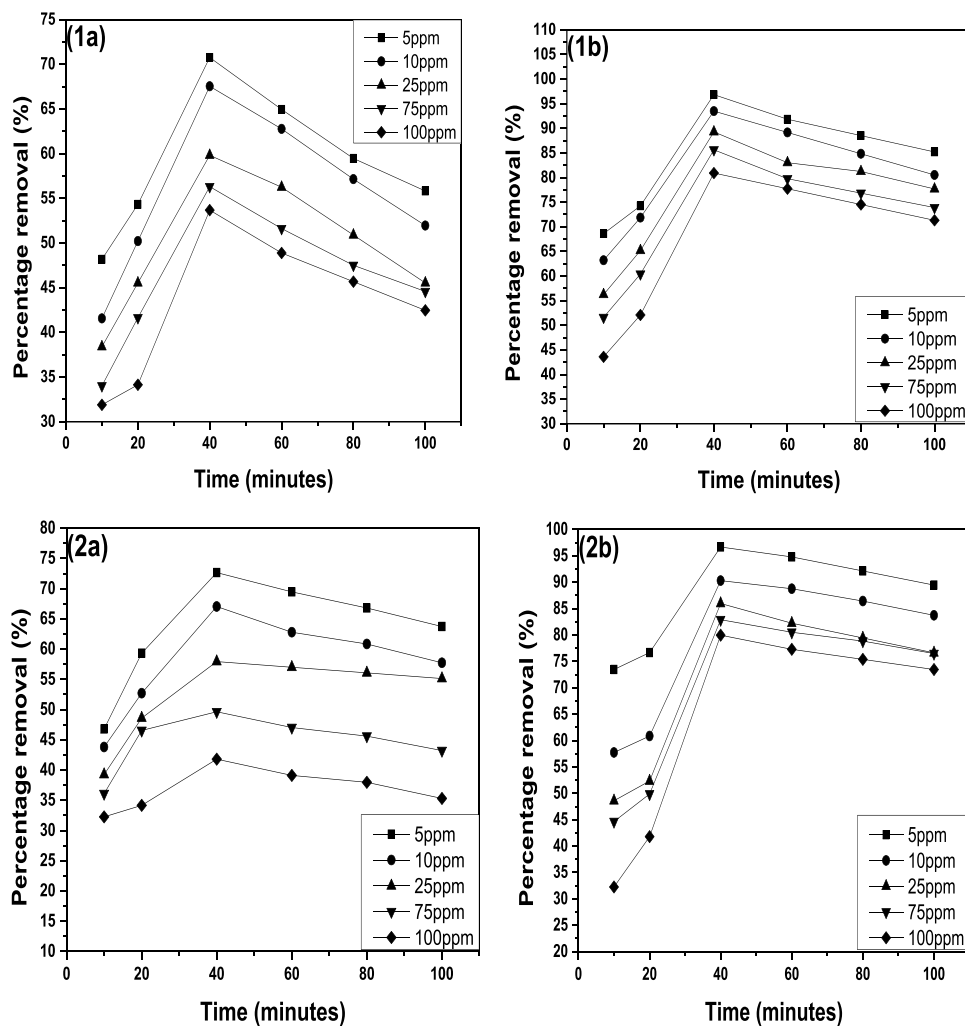
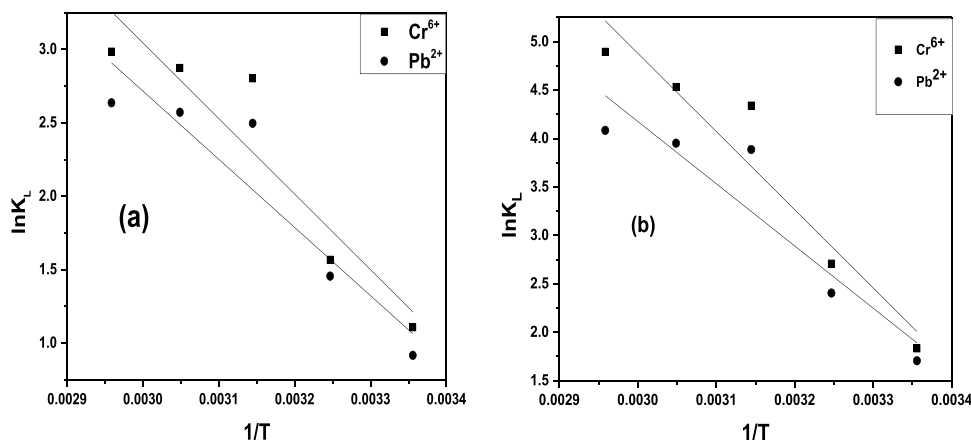


Fig. 12 Van't Hoff plot for Cr⁶⁺ and Pb²⁺ adsorption on Cu/Ni@rGO composites **a** without tungsten lamp and **b** with tungsten lamp



value of ΔG° was negative and also increased by increasing temperature. Increasing values of ΔG° under tungsten lamp and without tungsten lamp indicated the spontaneous nature of reaction between adsorbent and adsorbate. The value of ΔH° was positive in both cases that confirmed the best binding capabilities of adsorbent with adsorbates. ΔS° also had positive values which concerned about good affinity of contaminants (Pb²⁺ and Cr⁶⁺) with catalytic surface of synthesized nanocomposite.

Kinetics Models

Pseudo-first-order model stated that rate of sorption is directly linked with available number of free active sites. Due to adsorption of adsorbate, the heterogeneous surface of catalyst becomes smooth. For pseudo 1st order, plot was plotted between time (t) and $\ln(q_e - q_t)$ (Fig. 13). The R^2 value for this model is low as compared to the pseudo-2nd-order model which indicated that this model could not explain adsorption of cations onto composite (Table 3).

While in the case of pseudo 2nd order, graph was plotted between time (t) and t/q_t (Fig. 14). Parameters

calculated from this model are given in Table 3 which indicated that the best fitted model was pseudo 2nd order as the R^2 value was near to unity for this model.

Isotherm Models

The interaction of adsorbent with adsorbate and reaction mechanism was well explained by isotherm models. To confirm the best fitted model, three sorption isotherm models were employed on experimental data [68].

Langmuir isotherm depicted about monolayer formation of adsorbents on catalytic surface with uniform energy. From slope and intercept values of q_m and K_L were calculated (Fig. 15). Calculated values are given in Table 4. R^2 for this model was 0.96 for both cations under tungsten lamp; that is why this model could not explain adsorption phenomenon. The value of R_L is less than 1 so adsorption of both cations on catalytic surface is considered favorable.

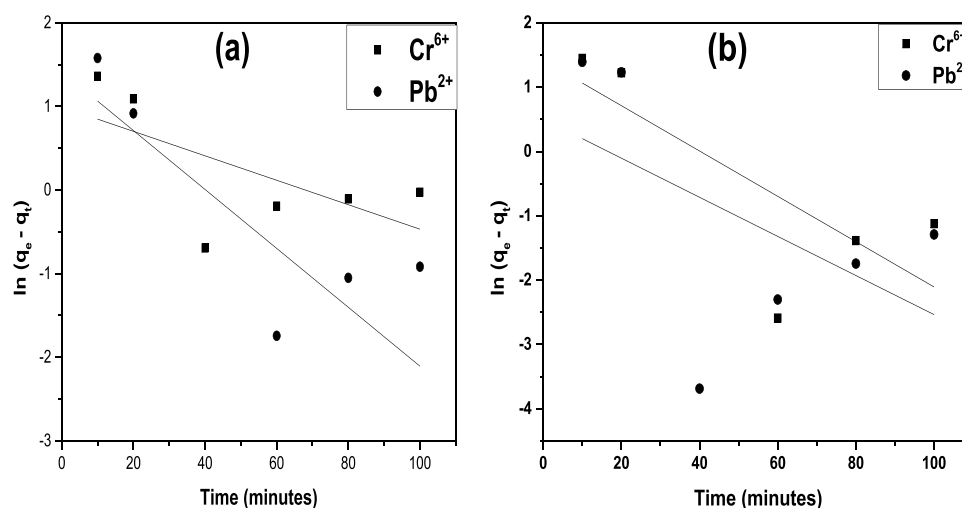
A graph between $\ln q_e$ vs. $\ln C_e$ was plotted as shown in Fig. 16 for determination of Freundlich isotherm parameters (n and K_f). The value of n calculated by Freundlich model

Table 1 Thermodynamics parameter without tungsten lamp

Adsorbing material	Contaminant	Temp (K)	K_L	ΔH° (kJ mol ⁻¹)	ΔS° (Jmol ⁻¹ K ⁻¹)	ΔG° (kJ mol ⁻¹)	R^2
Cu/Ni/Gr composite	Chromium	298	3.02	42.82	153.78	-2.74	0.82
		308	4.79			-4.01	
		318	16.5			-7.41	
		328	17.69			-7.83	
		338	19.77			-8.38	
	Lead	298	2.5	3.83	138.43	-2.27	
		308	4.28			-3.72	
		318	12.14			-6.60	
		328	13.08			-7.01	
		338	13.95			-7.40	

Table 2 Thermodynamic parameters under tungsten lamp

Adsorbing material	Contaminant	Temp (K)	K_L	ΔH° (kJ mol ⁻¹)	ΔS° (Jmol ⁻¹ K ⁻¹)	ΔG° (kJ mol ⁻¹)	R^2	
Cu/Ni/Gr composite	Chromium	298	6.25	7.21	242.03	-4.54	0.89	
		308	15		-6.93			
		318	76.66		-11.47			
		328	92.95		-12.35			
		338	133.61		-13.75			
	Lead	298	5.5		195.03	-4.22		0.82
		308	11.07		-6.15			
		318	48.75		-10.27			
		328	52.04		-10.77			
		338	59.40		-11.47			

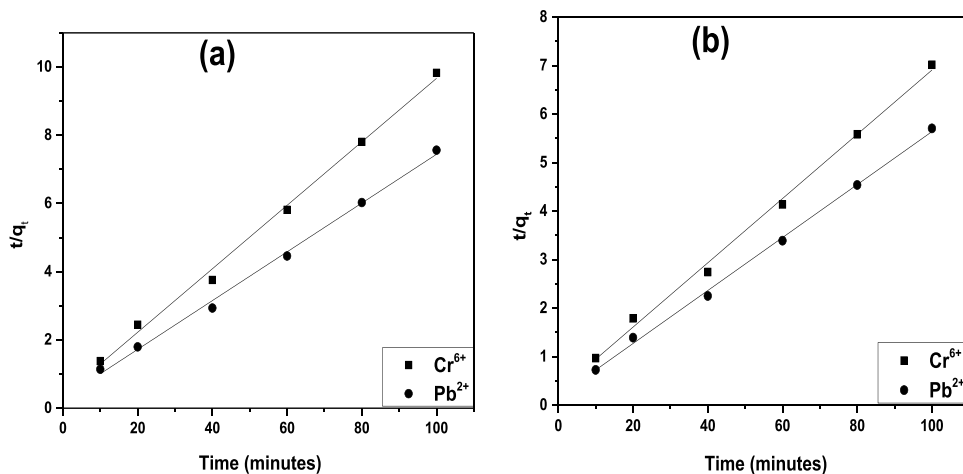
Fig. 13 Pseudo 1st order for Cr⁶⁺ and Pb²⁺ **a** without lamp and **b** with lamp**Table 3** Calculated parameters of kinetic adsorption of Cr⁶⁺ and Pb²⁺ on Cu/Ni@rGO composite

Kinetics models	Constants values	Without tungsten lamp		With tungsten lamp	
		Contaminants		Contaminants	
		Chromium	Lead	Chromium	Lead
Pseudo 1st order	R^2	0.25	0.58	0.46	0.09
	q_e	2.70	4.07	4.12	1.65
	K_1 (min ⁻¹)	-0.0001	-0.0003	-0.0003	-0.0003
Pseudo 2nd order	R^2	0.99	0.99	0.99	0.99
	q_e	1.44	1.34	1.33	1.19
	K_2 (min ⁻¹)	0.0009	0.0007	0.0006	0.0005

was less than 1 (Table 4) which confirmed that adsorption procedure of cations onto nanocomposite was physical in nature. The R^2 value was calculated 0.97 which is near to unity in case of Freundlich isotherm, so it was considered the best fitted model of adsorption mechanism between cations and synthesized nanocomposite.

The Temkin isotherm considers the indirect interactions between adsorbate and adsorbent assuming drop of heat of adsorption linearly instead of logarithmic while discounting very low and high concentration. It also presumes uniform distribution of binding energy. R^2 value 0.96 (Table 4) indicated weak interactions between adsorbent and adsorbate (Fig. 17).

Fig. 14 Pseudo 2nd order for Cr^{6+} and Pb^{2+} **a** without lamp and **b** with lamp



Error Analysis

Error analysis was applied on linear regression of adsorption isotherms with three error parameters, reduced Chi-Sqr (χ^2), residual sum of squares (SSE), and root-MSE (SD or

RMSE) Tables 5 and 6. Standard normalized error (SNE) was also calculated from these errors, and its lowest value with Freundlich isotherm proves its best fitted adsorption for both cations. [69].

Fig. 15 Langmuir isotherms for Cr^{6+} **1a** with lamp and **1b** without lamp. Langmuir isotherms for Pb^{2+} **2a** with lamp and **2b** without lamp

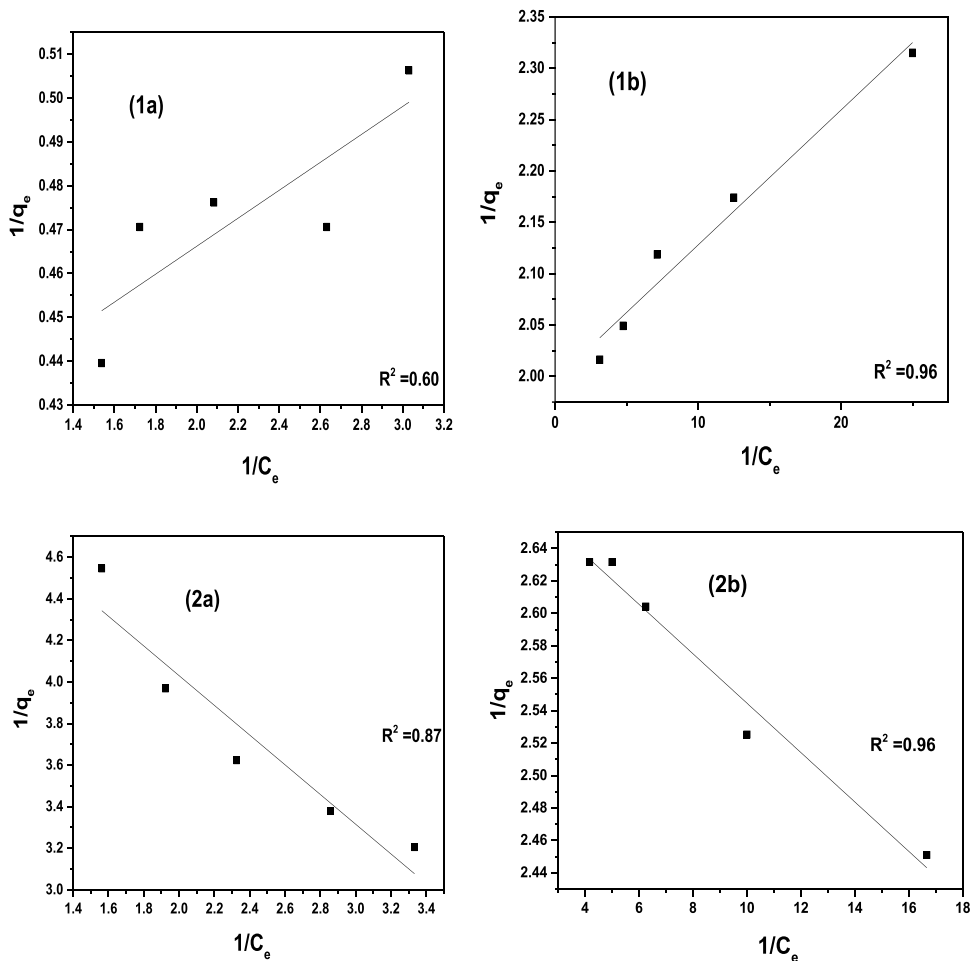


Table 4 Calculated values of isotherms with Cu/Ni@rGO nanocomposites

Isotherm models	Constants	Without tungsten lamp		Under tungsten lamp	
		Contaminants		Contaminants	
		Chromium	Lead	Chromium	Lead
Langmuir	Intercept	0.40	5.45	1.99	2.69
	Slope	0.03	0.71	0.013	0.01
	K_L (L/g)	12.61	0.25	151.94	24.34
	q_m (mg/g)	2.48	0.18	0.50	0.37
	R_L	0.05	0.17	0.006	0.05
	R^2	0.60	0.87	0.96	0.96
Freundlich	Intercept	0.37	0.73	0.26	0.45
	Slope	0.14	0.45	0.06	0.05
	$1/n$	0.14	0.45	0.06	0.05
	K_f	2.37	0.18	0.53	0.34
	R^2	0.60	0.97	0.97	0.97
	Temkin	Intercept	2.35	0.17	0.53
Slope		0.13	0.11	0.03	0.02
BT ($J\ mol^{-1}$)		0.31	0.11	0.03	0.02
Kr ($L\ mg^{-1}$)		1750.18	0.23	3528	9.69
R^2		0.60	0.96	0.96	0.96

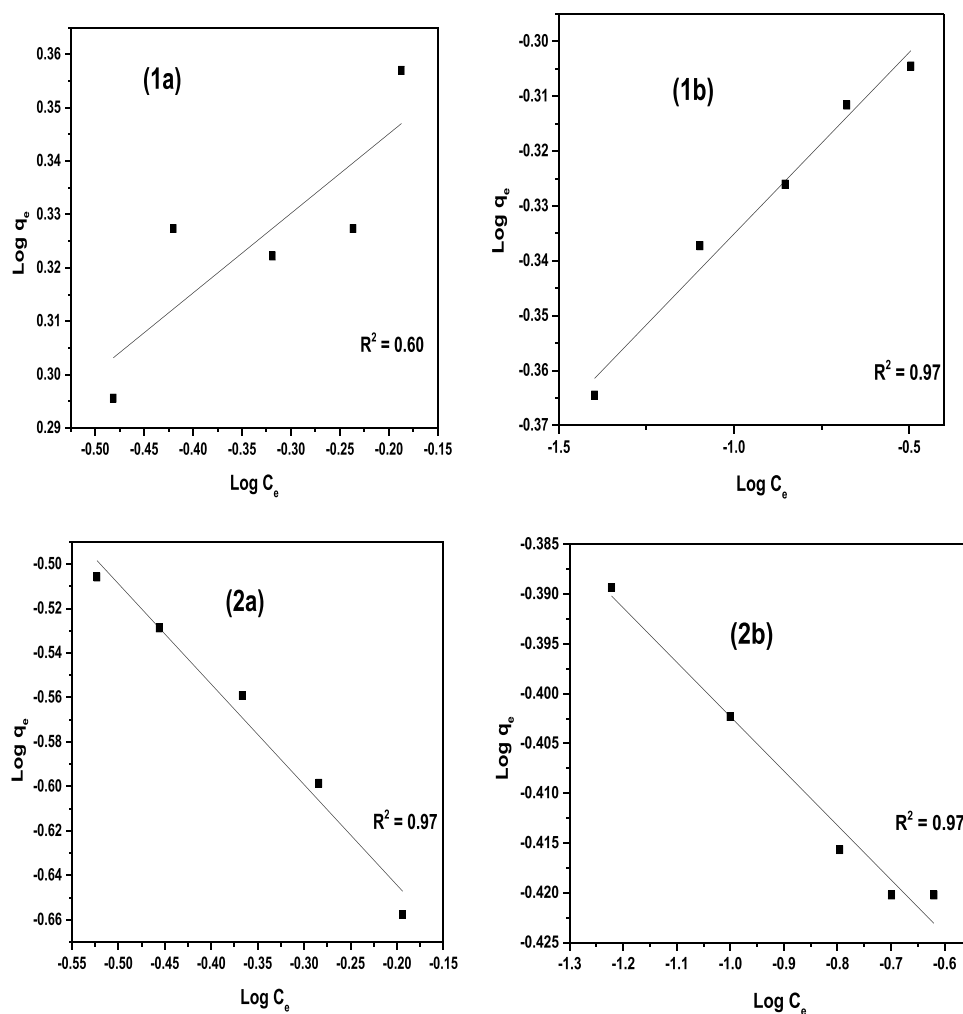
Fig. 16 Freundlich isotherms for Cr^{6+} **1a** with lamp and **1b** without lamp. Freundlich isotherms for Pb^{2+} **2a** with lamp and **2b** without lamp

Fig. 17 Temkin isotherms for Cr^{6+} **1a** with lamp and **1b** without lamp. Temkin isotherms for Pb^{2+} **2a** with lamp and **2b** without lamp

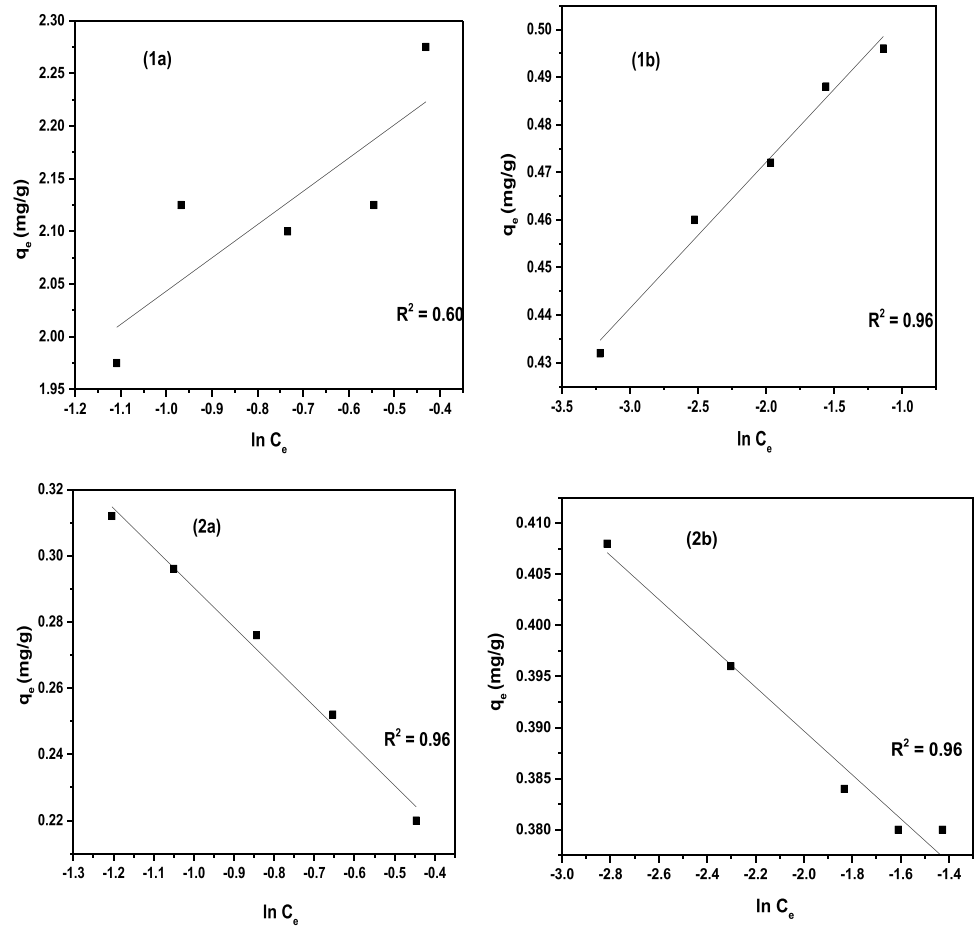


Table 5 Error analysis parameters

Isotherm models	Linear regression			
	Error parameters of chromium			
	Reduced Chi-Sqr	Root-MSE (SD) (RMSE)	Residual sum of squares (SSE)	Standard error of normalized error (SNE)
Langmuir	$5.44791E-4$	0.02334	0.00163	0.010424
Freundlich	$1.36884E-5$	0.0037	$4.10651E-5$	0.001655
Temkin	$1.23227E-5$	0.00351	$3.6968E-5$	0.00157

Table 6 Error analysis parameters

Isotherm models	Linear regression			
	Error parameters of lead			
	Reduced Chi-Sqr	Root-MSE (SD) (RMSE)	Residual sum of squares (SSE)	Standard error of normalized error (SNE)
Langmuir	$1.87903E-4$	0.01371	$5.6371E-4$	0.006131
Freundlich	$5.31245E-6$	0.0023	$1.59373E-5$	0.001029
Temkin	$4.55053E-6$	0.00213	$1.36516E-5$	0.00953

Recyclability

Regeneration and recyclability of a material are very important to observe its efficiency [70]. In the present work, synthesized Cu/Ni@rGO nanocomposite was regenerated about 5 times and percentage removal efficiency found to be decreased in each cycle by 3 to 5% as shown in Fig. 18 which depicted the stability and efficiency of synthesized material. The whole experiment was performed by adding 10 mg adsorbent in 25 mL binary mixture of cations, and the solution was kept on orbital shaker to achieve equilibrium for 2 h. After the 1st cycle, desorption was done by 0.1 M HCl and 0.1 M NaOH. For desorption, nanocomposite was agitated with acidic and basic solution for 10 min.

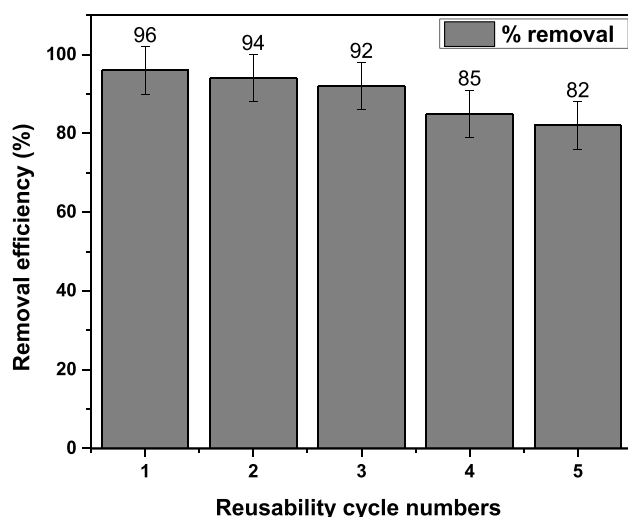


Fig. 18 Reusability of Cu/Ni@rGO composite

During each cycle, % removal efficiency was decreased as 96% > 94% > 92% > 85% > 82%. The comparison of synthesized material with previous reported nanomaterials to remove Cr⁶⁺ and Pb²⁺ is given in Table 7.

Conclusion

By using aqueous extract of *Ricinus communis* plant, Cu/Ni@rGO nanocomposite was successfully synthesized. Confirmation of synthesis, information about functional groups, structural morphology, elemental composition, and size were analyzed by UV-visible, FTIR, SEM, EDX, and XRD analysis. During removal of heavy metal ions in a single step, various factors were optimized like adsorbent dosage, cation solution concentration, pH, temperature, contact time, and % removal of Pb²⁺ and Cr⁶⁺ were recorded up to 94% under tungsten lamp as tungsten lamp source subsidized the separation of charges and decreased the recombination rates; therefore, maximum % removal was seen. Thermodynamics revealed the endothermic and spontaneous nature of reaction. Due to higher R^2 value (0.99), pseudo 2nd order was considered the best fitted model of kinetics for adsorption mechanism. It was concluded that multilayer adsorbent formation with non-uniform energy distribution occurred that corresponded to the Freundlich isotherm and revealed that the process was physisorption. Three error parameters, reduced Chi-Sqr (χ^2), residual sum of squares (SSE), and root-MSE (SD or RMSE), and standard normalized error (SNE) were calculated. For Freundlich isotherm, SNE value was the lowest that also proved its fitness to the adsorption mechanism. A small change in adsorption efficiency of Cu/Ni@rGO nanocomposite was observed even after five cycles.

Table 7 Comparison of different nanomaterials to remove Cr⁶⁺ and Pb²⁺

Absorbing nanomaterial	Methodology	Light source	Contaminants	Removal efficiency (%)	Removal time	Reference
CuO nanoparticles	Green methodology (<i>Capparis Spinosa</i>)	UV light	Pb ²⁺ and Cr ⁺³	97% (Pb ⁺²) 94% (Cr ⁺³)	90 min	[52]
Magnetite nanospheres	Solvothermal method	Visible	Cr ⁺⁶ and Pb ⁺²	70% (Pb ⁺²) 69% (Cr ⁺⁶)	10 min	[53]
Flamboyant pod activated carbon (FPAC)	Green methodology (<i>Delonix regia</i>)	UV light	Cr ⁺⁶ and Pb ⁺²	98% (Pb ⁺²) 94% (Cr ⁺⁶)	20–30 min	[54]
L-Cysteine functionalized magnetite nanoparticles (L-Cyst-Fe ₃ O ₄ NPs)	Co-precipitation method	Visible	Cr ⁺⁶ and Pb ⁺²	99% (Pb ⁺²) 96% (Cr ⁺⁶)	25–30 min	[55]
Orange peel/selenium (OP/Se)	Chemical precipitation/ reduction method	Visible	Cr ⁺⁶ and Pb ⁺²	99% (Pb ⁺²) 95% (Cr ⁺⁶)	60 min	[56]
Cu/Ni@rGO nanocomposite	Green methodology (<i>Ricinus communis</i>)	Tungsten lamp	Cr ⁺⁶ and Pb ⁺²	95% (Pb ⁺²) 96% (Cr ⁺⁶)	40 min	Present work

Supplementary Information The online version contains supplementary material available at <https://doi.org/10.1007/s11468-024-02461-8>.

Author Contributions Amina Kanwal: research planning, experimental investigation and manuscript writing. Tayyaba Shahzadi: support of materials synthesis, project supervision and manuscript review. Tauheeda Riaz, Maria Zaib: support of instrumentation and manuscript review.

Funding There was not any funding involved in this reported research work.

Data Availability All data that support the findings of this study is contained within the article.

Declarations

Ethics Approval It is declared that neither human nor animal was involved for conduction of this research work.

Competing Interests The authors declare no competing interests.

References

- Osman AI, El-Monaem EMA, Elgarahy AM, Aniagor CO, Hosny M, Farghali M, Rashad E, Ejimofor MI, López-Maldonado EA, Ihara I, Yap PS, Rooney DW, Eltaweil AS (2023) Methods to prepare biosorbents and magnetic sorbents for water treatment. *Environ Chem Lett* 21(1):2337–2398. <https://doi.org/10.1007/s10311-023-01603-4>
- Angraal S, Krumholz HM, Schulz WL (2017) Blockchain technology. *Circ Cardiovasc Qual Outcomes* 10:31–21. <https://doi.org/10.1161/circoutcomes.117.003800>
- Polis HB, Harmsen GH (1994) Industrial wastewater treatment today and tomorrow. *Water Sci Technol* 30:109–117. <https://doi.org/10.2166/wst.1994.0076>
- Shahzadi T, Kanwal A, Jabeen H, Riaz T, Zaib M (2021) Eco-friendly synthesis of silver nanoparticles using *gazania rigens* and evaluation of activities. *Environ Eng Manage J* 20(4):43–52. <https://doi.org/10.30638/eemj.2021.005>
- Dotaniya ML, Thakur JK, Meena VD, Jajoria DK, Rathor G (2014) Chromium pollution a threat to environment—a review. *Agric Rev* 35:153. <https://doi.org/10.5958/0976-0741.2014.00094.4>
- Yoshinaga M, Ninomiya H, Hossain MMAA, Sudo M, Akhand AA, Ahsan N, Alim MdA, Khalequzzaman Md, Iida M, Yajima I, Ohgami N, Kato M (2018) A comprehensive study including monitoring, assessment of health effects and development of a remediation method for chromium pollution. *Chemosphere* 201:667–675. <https://doi.org/10.1016/j.chemosphere.2018.03.026>
- Hossini H, Shafie B, Niri AD, Nazari M, Esfahlan AJ, Ahmadpour M, Nazmara Z, Ahmadimanesh M, Makhdomi P, Mirzaei N, Hoseinzadeh E (2022) A comprehensive review on human health effects of chromium: insights on induced toxicity. *Environ Sci Pollut Res Int* 29(6):70686–70705. <https://doi.org/10.1007/s11356-022-22705-6>
- Shahzadi T, Rehman S, Riaz T, Zaib M (2020) Eco-friendly synthesis of ZnO nanoparticles using *Cannabis sativa* and assessment of its activities as efficient dyes removal and antioxidant agent. *Int J Environ Anal Chem* 102:4738–4756. <https://doi.org/10.1080/03067319.2020.1789610>
- Beattie AD, Moore MR, Devenay WT, Miller AR, Goldberg A (1972) Environmental lead pollution in an urban soft-water area. *BMJ* 2(3):491–493. <https://doi.org/10.1136/bmj.2.5812.491>
- Sharma S, Bhattacharya A (2016) Drinking water contamination and treatment techniques. *Appl Water Sci* 7:1043–1067. <https://doi.org/10.1007/s13201-016-0455-7>
- Ekpo A, Amayo J (2008) Determination of lead, cadmium and mercury in surrounding water and organs of some species of fish from Ikpoba river in Benin city, Nigeria. *Int J Phys Sci* 3(1):289–292. <https://doi.org/10.5897/ijps.9000161>
- Triantafyllidou S, Nguyen CK, Zhang Y, Edwards MA (2012) Lead (Pb) quantification in potable water samples implications for regulatory compliance and assessment of human exposure. *Environ Monit Assess* 185:1355–1365. <https://doi.org/10.1007/s10661-012-2637-6>
- Gupta N, Amritphale SS, Chandra N (2010) Removal of Zn (II) from aqueous solution by using hybrid precursor of silicon and carbon. *Bioresour Technol* 101:3355–3362. <https://doi.org/10.1016/j.biortech.2009.12.024>
- Zhang Y, Yuan S, Feng X, Li H, Zhou J, Wang B (2016) Preparation of nanofibrous metal–organic framework filters for efficient air pollution control. *J Am Chem Soc* 138:5785–5788. <https://doi.org/10.1021/jacs.6b02553>
- Bezerra BGP, Parodia A, Da Silva DR, Pergher SBC (2019) Cleaning produced water a study of cation and anion removal using different adsorbents. *J Environ Chem Eng* 7:103006. <https://doi.org/10.1016/j.jece.2019.103006>
- Velazquez-Jimenez LH, Pavlick A, Rangel-Mendez JR (2013) Chemical characterization of raw and treated agave bagasse and its potential as adsorbent of metal cations from water. *Ind Crops Prod* 43:200–206. <https://doi.org/10.1016/j.indcrop.2012.06.049>
- Kanwal A, Shahzadi T, Riaz T (2024) Sustainable degradation of binary dye mixtures using Fe/Co/rGO nanocomposite: dual dye dynamics, adsorption and reusability. *Arab J Sci Eng*. <https://doi.org/10.1007/s13369-024-09274-1>
- Wadhawan S, Jain A, Nayyar J, Mehta SK (2020) Role of nanomaterials as adsorbents in heavy metal ion removal from waste water. *J Water Process Eng* 33:101038. <https://doi.org/10.1016/j.jwpe.2019.101038>
- Zhang Y-R, Wang S-Q, Shen S-L, Zhao B-X (2013) A novel water treatment magnetic nanomaterial for removal of anionic and cationic dyes under severe condition. *Chem Eng J* 233:258–264. <https://doi.org/10.1016/j.cej.2013.07.009>
- Sarma GK, Gupta SS, Bhattacharyya KG (2019) Nanomaterials as versatile adsorbents for heavy metal ions in water: a review. *Environ Sci Pollut Res Int* 26:6245–6278. <https://doi.org/10.1007/s11356-018-04093-y>
- Liu X, Ma R, Wang X, Ma Y, Yang Y, Zhuang L, Zhang S, Jehan R, Chen J, Wang X (2019) Graphene oxide-based materials for efficient removal of heavy metal ions from aqueous solution. *Environ Pollut* 252:62–73. <https://doi.org/10.1016/j.envpol.2019.05.050>
- Fu W, Huang Z (2018) Magnetic dithiocarbamate functionalized reduced graphene oxide for the removal of Cu(II), Cd(II), Pb(II), and Hg(II) ions from aqueous solution: synthesis, adsorption, and regeneration. *Chemosphere* 209:449–456. <https://doi.org/10.1016/j.chemosphere.2018.06.087>
- Weng X, Wu J, Ma L, Owens G, Chen Z (2019) Impact of synthesis conditions on Pb(II) removal efficiency from aqueous solution by green tea extract reduced graphene oxide. *Chem Engin J* 359:976–981. <https://doi.org/10.1016/j.cej.2018.11.089>
- Wang X, Liu Y, Pang H, Yu S, Ai Y, Ma X, Song G, Hayat T, Alsaedi A, Wang X (2018) Effect of graphene oxide surface modification on the elimination of Co(II) from aqueous solutions. *Chem Engin J* 344:380–390. <https://doi.org/10.1016/j.cej.2018.03.107>

25. Zheng Y, Cheng B, You W, Yu J, Ho W (2019) 3D hierarchical graphene oxide-NiFe LDH composite with enhanced adsorption affinity to Congo red, methyl orange and Cr(VI) ions. *J Hazard Mater* 369:214–225. <https://doi.org/10.1016/j.jhazmat.2019.02.013>
26. Pakulski D, Włodzimierz C, Samanta W, Alessandro A, Piotr P, Violetta P, Artur C, Paolo S (2018) Graphene oxide-branched polyethylenimine foams for efficient removal of toxic cations from water. *J Mater Chem* 6(20):9384–9390. <https://doi.org/10.1039/C8TA01622D>
27. Ramesha GK, Kumara AV, Muralidhara HB, Sampath S (2011) Graphene and graphene oxide as effective adsorbents toward anionic and cationic dyes. *JCIS* 361:270–277. <https://doi.org/10.1016/j.jcis.2011.05.050>
28. Wan S, Ding W, Wang Y, Wu J, Gu Y, He F (2018) Manganese oxide nanoparticles impregnated graphene oxide aggregates for cadmium and copper remediation. *Chem Eng J* 350:1135–1143. <https://doi.org/10.1016/j.cej.2018.06.068>
29. Mishra AK, Ramaprabhu S (2011) Functionalized graphene sheets for arsenic removal and desalination of sea water. *Desalination* 282:39–45. <https://doi.org/10.1016/j.desal.2011.01.038>
30. Wojtoniszak M, Zielinska B, Chen X, Kalenczuk RJ, Borowiak-Palen E (2011) Synthesis and photocatalytic performance of TiO₂ nanospheres–graphene nanocomposite under visible and UV light irradiation. *J Mater Sci* 47:3185–3190. <https://doi.org/10.1126/science.1102896>
31. Ma HL, Zhang Y, Hu QH, Yan D, Yu ZZ, Zhai M (2012) Chemical reduction and removal of Cr(vi) from acidic aqueous solution by ethylenediamine-reduced graphene oxide. *J Mater Chem* 22:5914. <https://doi.org/10.1039/C2JM00145D>
32. Gusain R, Kumar N, Ray SS (2020) Recent advances in carbon nanomaterial-based adsorbents for water purification. *Coord Chem Rev* 405:213111. <https://doi.org/10.1016/j.ccr.2019.213111>
33. Li J, Zeng H, Zeng Z, Zeng Y, Xie T (2021) Promising graphene-based nanomaterials and their biomedical applications and potential risks: a comprehensive review. *ACS* 7(12):5363–5396. <https://doi.org/10.1021/acsbio.1c00875>
34. Singh S, Hasan MR, Sharma P, Narang J (2022) Graphene nanomaterials: the wondering material from synthesis to applications. *Sens Int* 3:100190. <https://doi.org/10.1016/j.sintl.2022.100190>
35. Cellot G, Franceschi BA, Ballerini L (2022) Nanomedicine and graphene-based materials: advanced technologies for potential treatments of diseases in the developing nervous system. *Pediatr Res* 92(1):71–79. <https://doi.org/10.1021/acsomega.0c00450>
36. Kumar M (2017) A review on phytochemical constituents and pharmacological activities of Ricinus communis L. plant. *Int J Pharmacogn Phytochem Res* 9:376–376. <https://doi.org/10.25258/phyto.v9i4.8116>
37. Nasrollahzadeh M, Sajjadi M, Komber H, Khonakdar HA, Sajadi SM (2019) In situ green synthesis of Cu-Ni bimetallic nanoparticles supported on reduced graphene oxide as an effective and recyclable catalyst for the synthesis of N-benzyl-N-aryl-5-amino-1H-tetrazoles. *Appl Organomet Chem* 33:56–37. <https://doi.org/10.1002/aoc.4938>
38. Kanwal A, Shahzadi T, Riaz T, Zaib M, Khan S, Habila MA, Silanpaa M (2023) Photocatalytic degradation studies of organic dyes over novel Cu/Ni loaded reduced graphene oxide hybrid nanocomposite adsorption, kinetics and thermodynamic studies. *Molecules* 28:6474–6474. <https://doi.org/10.3390/molecules28186474>
39. Elreedy A, Ibrahim E, Hassan N, El-Dissouky A, Fujii M, Yoshimura C, Tawfik A (2017) Nickel-graphene nanocomposite as a novel supplement for enhancement of biohydrogen production from industrial wastewater containing mono-ethylene glycol. *Energy Convers Manage* 140:133–144. <https://doi.org/10.1016/j.enconman.2017.02.080>
40. Zaaba NI, Foo KL, Hashim U, Tan SJ, Liu WW, Voon CH (2017) Synthesis of graphene oxide using modified hummers method solvent influence. *Procedia Eng* 184:469–477. <https://doi.org/10.1016/j.proeng.2017.04.118>
41. Kosmulski M (2018) The pH dependent surface charging and points of zero charge. *Adv Colloid Interface Sci* 251:115–138. <https://doi.org/10.1016/j.cis.2017.10.005>
42. Kosmulski M (2009) pH-dependent surface charging and points of zero charge. *Adv Colloid Interface Sci* 337:439–448. <https://doi.org/10.1016/j.jcis.2009.04.072>
43. Santos PM, Batista DLJ, Ribeiro LAF (2018) Identification of antioxidant and antimicrobial compounds from the oilseed crop Ricinus communis using a multiplatform metabolite profiling approach. *Ind Crops and Prod* 124:834–844. <https://doi.org/10.1016/j.indcrop.2018.08.061>
44. Rocha FS, Gomes AJ, Lunardi CN, Kaliaguine S, Patience GS (2018) Experimental methods in chemical engineering ultraviolet visible spectroscopy. *Can J Chem Eng* 96:2512–2517. <https://doi.org/10.1002/cjce.23344>
45. Andrijanto E, Shoelarta S, Subiyanto G, Rifki S (2016) Facile synthesis of graphene from graphite using ascorbic acid as reducing agent. *AIP Conf Proc* 4:6577–7621. <https://doi.org/10.1063/1.4945457>
46. Xiong G, Pal U, Serrano JG, Ucer KB, Williams RT (2006) Photoluminescence and FTIR study of ZnO nanoparticles the impurity and defect perspective. *PSS Conf Crit Rev* 3:3577–3581. <https://doi.org/10.1002/pssc.200672164>
47. Hidayah NMS, Liu W-W, Lai CW (2017) Comparison on graphite, graphene oxide and reduced graphene oxide: synthesis and characterization. *AIP Conf Proc* 4:6577–7621. <https://doi.org/10.1063/1.5005764>
48. Hassanzadeh-Tabrizi SA (2023) Precise calculation of crystallite size of nanomaterials a review. *J Alloys Compd* 968:171914. <https://doi.org/10.1016/j.jallcom.2023.171914>
49. Dudkiewicz A, Tiede K, Loeschner K, Jensen LHS, Jensen E, Wierzbicki R, Boxall ABA, Molhave K (2011) Characterization of nanomaterials in food by electron microscopy. *Trends Anal Chem* 30:28–43. <https://doi.org/10.1016/j.trac.2010.10.007>
50. Laborda F, Bolea E, Cepriá G, Navarro L, Morón J, Pérez-Arantegui J, Castillo JR (2016) Detection, characterization and quantification of inorganic engineered nanomaterials a review of techniques and methodological approaches for the analysis of complex samples. *Anal Chim Acta* 904:10–32. <https://doi.org/10.1016/j.aca.2015.11.008>
51. Joshi KM, Shrivastava VS (2011) Photocatalytic degradation of chromium (VI) from wastewater using nanomaterials like TiO₂, ZnO, and CdS. *Appl Nanosci* 1:147–155. <https://doi.org/10.1007/s13204-011-0023-2>
52. Ahmadi A, Heidarzadeh S, Mokhtari AR, Darezereshki E, Harouni HA (2014) Optimization of heavy metal removal from aqueous solutions by maghemite (γ-Fe₂O₃) nanoparticles using response surface methodology. *J Geochem Explor* 147:151–158. <https://doi.org/10.1016/j.gexplo.2014.10.005>
53. Fakhar N, Khan SA, Siddiqi WA, Khan TA (2022) Investigating the sequestration potential of a novel biopolymer-modified ceria/montmorillonite nanocomposite for chromium and coomassie brilliant blue from the aqueous phase equilibrium and kinetic studies. *Environ Sci Adv* 1:558–569. <https://doi.org/10.1039/d2va00125j>
54. Eshraghi F, Nezamzadeh-Ejhieh A (2018) EDTA-functionalized clinoptilolite nanoparticles as an effective adsorbent for Pb(II) removal. *Environ Sci Pollut Res International* 25:14043–14056. <https://doi.org/10.1007/s11356-018-1461-0>
55. Lung I, Stan M, Opris O, Soran ML, Senila M, Stefan M (2018) Removal of lead(II), cadmium(II), and arsenic(III) from aqueous

- solution using magnetite nanoparticles prepared by green synthesis with Box-Behnken design. *Anal Lett* 51:2519–2531. <https://doi.org/10.1080/00032719.2018.1446974>
56. Giraldo L, Erto A, Moreno-Piraján JC (2013) Magnetite nanoparticles for removal of heavy metals from aqueous solutions: synthesis and characterization. *Adsorption* 19:465–474. <https://doi.org/10.1007/s10450-012-9468-1>
 57. Dargahi A, Gholestanifar H, Darvishi P, Karami A, Hasan SH, Poormohammadi A, Behzadnia A (2016) An investigation and comparison of removing heavy metals lead and chromium from aqueous solutions using magnesium oxide nanoparticles. *Pol J Environ Stud* 25:557–562. <https://doi.org/10.15244/pjoes/60281>
 58. Gupta VK, Chandra R, Tyagi I, Verma M (2016) Removal of hexavalent chromium ions using CuO nanoparticles for water purification applications. *J Colloid Interface Sci* 478:54–62. <https://doi.org/10.1016/j.jcis.2016.05.064>
 59. Nematollahzadeh A, Seraj S, Mirzayi B (2015) Catecholamine coated maghemite nanoparticles for the environmental remediation hexavalent chromium ions removal. *Chem Eng J* 277:21–29. <https://doi.org/10.1016/j.cej.2015.04.135>
 60. Shahzadi T, Anwaar A, Riaz T, Zaib M (2022) Sulfate and phosphate ions removal using novel nano-adsorbents modeling and optimization, kinetics, isotherm and thermodynamic studies. *Int J Phytoremed* 24:1518–1532. <https://doi.org/10.1080/15226514.2022.2040421>
 61. Zhu S, Huang X, Wang D (2018) Enhanced hexavalent chromium removal performance and stabilization by magnetic iron nanoparticles assisted biochar in aqueous solution mechanisms and application potential. *Chemosphere* 207:50–59. <https://doi.org/10.1016/j.chemosphere.2018.05.046>
 62. Hosseini R, Sayadi MH, Shekari H (2019) Adsorption of nickel and chromium from aqueous solutions using copper oxide nanoparticles adsorption isotherms, kinetic modeling, and thermodynamic studies. *Avicenna J Environ Health Eng* 6:66–74. <https://doi.org/10.34172/ajehe.2019.09>
 63. Aslani H, Kosari TE, Naseri S, Nabizadeh R, Khazaei M (2018) Hexavalent chromium removal from aqueous solution using functionalized chitosan as a novel nano-adsorbent modeling and optimization, kinetic, isotherm, and thermodynamic studies, and toxicity testing. *Environ Sci Pollut Res Int* 25:20154–20168. <https://doi.org/10.1007/s11356-018-2023-1>
 64. Singh R, Bhatia R (2020) Experimental and modeling process optimization of lead adsorption on magnetite nanoparticles via isothermal, kinetics, and thermodynamic studies. *ACS Omega* 5:10826–10837. <https://doi.org/10.1021/acsomega.0c00450>
 65. Shahzadi T, Sanaullah S, Riaz T, Zaib M, Kanwal A, Jabeen H (2021) Kinetics and thermodynamic studies of organic dyes removal on adsorbent developed from Viola tricolor extract and evaluation of their antioxidant activity. *Environ Dev Sustain* 23:17923–17941. <https://doi.org/10.1007/s10668-021-01421-0>
 66. Mohamed AR, Hussein HH, Sirhan MM (2022) Removal lead (II) and chromium (III) Ions from aqueous solutions, by copper nanoparticles prepared using Capparis spinosa leaf extract. *IJHS* 8:9091–9106. <https://doi.org/10.53730/ijhs.v6ns4.11900>
 67. Kumari M, Pittman CU, Mohan D (2015) Heavy metals chromium (VI) and lead (II) removal from water using mesoporous magnetite (Fe₃O₄) nanospheres. *JCIS* 442:120–132. <https://doi.org/10.1016/j.jcis.2014.09.012>
 68. Mustapha SI, Adewoye LT, Aderibigbe FA, Mohammed Haji AMI, Adekola Tijani IA (2018) Removal of lead and chromium from aqueous solution onto flamboyant Delonix regia pod activated carbon. *Nig J Technol Dev* 14:56. <https://doi.org/10.4314/njtd.v14i2.4>
 69. Terdputtakun A, Arqueropanyo O-A, Sooksamiti P, Janhom S, Naksata W (2017) Adsorption isotherm models and error analysis for single and binary adsorption of Cd(II) and Zn(II) using leonardite as adsorbent. *Environ Earth Sci* 76:54. <https://doi.org/10.1007/s12665-017-7110-y>
 70. Aziz M, Aziz R, Rafiq MT, Abbasi M, Mehwish T, Muhammad UA, ElA A, Elesawy BH, Eed EM, Khalifa AS, Qayyum A (2022) Efficient removal of lead and chromium from aqueous media using selenium based nanocomposite supported by orange peel. *Front Environ Sci* 10:32. <https://doi.org/10.3389/fenvs.2022.947827>

Publisher's Note Springer Nature remains neutral with regard to jurisdictional claims in published maps and institutional affiliations.

Springer Nature or its licensor (e.g. a society or other partner) holds exclusive rights to this article under a publishing agreement with the author(s) or other rightsholder(s); author self-archiving of the accepted manuscript version of this article is solely governed by the terms of such publishing agreement and applicable law.